Eur. Phys. J. B **51**, 583–591 (2006)
DOI: 10.1140/epjb/e2006-00256-0

THE EUROPEAN PHYSICAL JOURNAL B

Acoustic phonon dynamics in strained cubic and hexagonal GaN/Al_2O_3 superlattices

P.D. Sesion Jr.[1], E.L. Albuquerque[1,a], M.S. Vasconcelos[2], P.W. Mauriz[2], and V.N. Freire[3]

[1] Departamento de Física, Universidade Federal do Rio Grande do Norte, 59072-970, Natal-RN, Brazil
[2] Departamento de Ciências Exatas, Centro Federal de Educação Tecnológica do Maranhão, 65025-001, São Luís-MA, Brazil
[3] Departamento de Física, Universidade Federal do Ceará, Campus do Pici, 60455-970, Fortaleza-CE, Brazil

Received 21 December 2005 / Received in final form 24 February 2006
Published online 28 June 2006 –

Abstract. We study the acoustic-phonon spectra in periodic and quasiperiodic (Fibonacci type) superlattices made up from III–V nitride materials (GaN) intercalated by sapphire (Al_2O_3). Due to the misalignments between the sapphire and the GaN layers that can lead to threading dislocation densities as high as 10^8-10^{10} cm^{-1}, and a significant lattice mismatch ($\sim$14%), the phonon dynamics is described beyond the continuum elastic model using coupled elastic and electromagnetic equations, stressing the importance of the piezoelectric polarization field in a strained condition. We use a transfer-matrix treatment to simplify the algebra, which would be otherwise quite complicated, allowing a neat analytical expressions for the phonon dispersion relation. Furthermore, a quantitative analysis of the localization and magnitude of the allowed band widths in the phonon's spectra, as well as their scale law and the parametric spectrum of singularities $f(\alpha)$, are presented and discussed.

PACS. 63.20.Pw Localized modes – 63.22.+m Phonons or vibrational states in low-dimensional structures and nanoscale materials – 68.65.Cd Superlattices – 71.55.Eq III-V semiconductors

1 Introduction

The III–V nitride materials, such as GaN, display important piezoelectric polarization fields in a strained condition and can crystallize in both hexagonal wurtzite or cubic zinc-blend structures [1]. The wurtzite crystals have a different unit cell structure (four atoms per unit cell with nine optical and three acoustic phonons for a given wavevector), as well as a lower symmetry when compared to the cubic zinc-blende counterpart, leading to a different carrier-phonon interaction. Although significant advances in growth, doping, and device applications of group III–V nitride materials have been achieved with their stable wurtzite hexagonal phase, less progress has been made with their metastable zinc-blend cubic structure. However, devices with a zinc-blend structure would have considerable advantages. This is particularly true for GaN due to its higher saturated electron drift velocity, easy cleavage, and lower band energy [2,3]. Also cubic nitrides are expected to have higher mobility, due to the decrease of the phonon number for the higher symmetry structure. Therefore, information on the vibrational properties of both structures (hexagonal and cubic) are strongly desirable.

The hexagonal wurtzite structures are uniaxial crystals with the optical axis coinciding with the Cartesian z-axis, which is perpendicular to the hexagons (forming the xy-plane). On the contrary to their hexagonal counterparts, the cubic structures can be grown free from modulation due to spontaneous polarization and strain-induced piezoelectric fields. The spatial separation of the carriers wave function, induced by the quantum-confined Stark effect in the hexagonal phase, is avoided in the cubic structure [4].

On the other hand, the discovery of quasiperiodic structures has fired up a new field of condensed-matter physics and given rise to many practical application (for an up to date review of this field see Refs. [5,6]). For example, the multiwavelength second-harmonic generation [7] and the direct third-harmonic generation [8] have been realized in a Fibonacci superlattice. In the field of photonic crystals, the complete photonic band gap in 12-fold symmetric quasicrystals has been recently reported [9].

It is our aim in this work to investigate the acoustic-phonon spectra in multilayer structures composed of

[a] e-mail: eudenilson@dfte.ufrn.br

hexagonal and cubic GaN layers, intercalated by an insulator material (Al_2O_3-sapphire), arranged in a periodical and quasiperiodic Fibonacci type fashion. It has been shown that in GaN films on sapphire substrates the misalignments between the sapphire base and the GaN layers can lead to threading dislocation densities as high as 10^8–10^{10} cm^{-2} [10], as well as a significant lattice mismatch (∼14%) [11], leading to the appearance of a strain-induced or piezoelectric polarization $\delta\vec{P}$ [12,13], given by

$$\delta P_i = e_{ijk} s_{jk} \tag{1}$$

besides the spontaneous polarization in the equilibrium superlattice structure. Here repeated subscript are summed over, ijk can be any Cartesian x, y, or z axis, e_{ijk} is the third rank piezoelectric tensor, and s_{kl}, the strain tensor, is defined by:

$$s_{jk} = (1/2)\left(\frac{\partial u_j}{\partial r_k} + \frac{\partial u_k}{\partial r_j}\right), \tag{2}$$

u_k being the displacement along the coordinate axes r_k.

Therefore the presence of this piezoelectric polarization component arising due to the lattice mismatch between GaN and sapphire, prevent us to use the much simpler continuum equation

$$\rho\partial^2 u_i/\partial t^2 = \partial S_{ij}/\partial r_j, \tag{3}$$

as in previous work [14], to describe the acoustic phonon dynamics. Instead, we should take into account the piezoelectric polarization field, whose elastic equation is coupled to the electromagnetic one (see next section). Previous work in this subject have considered transverse elastic waves in periodic [17,18] and quasiperiodic Fibonacci superlattice [15], considering layers of hexagonal symmetry and using the surface Green function matching method [16]. In equation (3), ρ is the density of the material (GaN), and S_{ij} is the stress tensor, given by $S_{ij} = C_{ijkl} s_{kl}$, where C_{ijkl} is the 4th-order elastic tensor. We consider also a transfer-matrix treatment to simplify the algebra, which would be otherwise quite complicated, that allows one to obtain a neat analytical expressions for the phonon dispersion relation. Furthermore, we perform also a quantitative analysis of the localization and magnitude of the allowed band widths in the acoustic phonon's spectra, their scale law and the parametric spectrum of singularities $f(\alpha)$.

The plan of this work is as follows: we start in Section 2 with our theoretical model along with some physical parameters definitions. The acoustic-phonon spectra for the periodic and quasiperiodic structures considered in this work are presented in Section 3. Further, in Section 4, we present their localization profiles and the connection with a fractal behavior through the scaling law of their bandwidth spectra as well as some concluding remarks.

2 General theory

We now present our theory to study the vibration modes in superlattices composed of zinc-blende (cubic) and wurtzite (hexagonal) GaN intercalated by sapphire, forming a binary superlattice structure, namely, /Al_2O_3/GaN/$\cdots$/substrate, where the substrate is here considered to be a transparent dielectric medium like vacuum.

Let us consider first the nitride layer GaN. The piezoelectric term responsible for the coupled elastic and electromagnetic fields is usually weak enough to allow the hybrid wave solution to behave like a *quasielastic* mode, with a phase velocity slightly lower than the uncoupled elastic mode, and a *quasielectromagnetic* mode, with a phase velocity shifted to a slightly higher value than the electromagnetic wave. As the electromagnetic wave has a velocity approximately five orders of magnitude higher than the elastic wave, we can describe the former in the static field approximation in which the particle displacement u_j ($j = x, y, z$) along the coordinate axes r_j is coupled, through the piezoelectric tensor e_{ijk}, to the electrical potential ϕ by the following set of equations [19]:

$$\rho\frac{\partial^2 u_j}{\partial t^2} - C_{ijkl}\frac{\partial^2 u_k}{\partial r_i \partial r_l} - e_{kij}\frac{\partial^2 \phi}{\partial r_i \partial r_k} = 0, \tag{4}$$

$$e_{ikl}\frac{\partial^2 u_k}{\partial r_i \partial r_l} - \epsilon_{ik}\frac{\partial^2 \phi}{\partial r_i \partial r_k} = 0, \tag{5}$$

where i, j, k and l can be x, y, or z with repeated subscript summed over. Also, ϵ_{ik} is the second rank dielectric permittivity tensor defined by:

$$\epsilon(\omega) = \begin{pmatrix} \epsilon_{xx} & 0 & 0 \\ 0 & \epsilon_{xx} & 0 \\ 0 & 0 & \epsilon_{zz} \end{pmatrix}. \tag{6}$$

Here ϵ_{xx} and ϵ_{zz} are the dielectric functions perpendicular and parallel to the z-axis, respectively. They are given by (neglecting any damping effect):

$$\epsilon_{xx} = \epsilon_\infty \frac{\omega^2 - \omega_{LO,E_1}^2}{\omega^2 - \omega_{TO,E_1}^2} \tag{7}$$

$$\epsilon_{zz} = \epsilon_\infty \frac{\omega^2 - \omega_{LO,A_1}^2}{\omega^2 - \omega_{TO,A_1}^2}, \tag{8}$$

where ϵ_∞ is the high-frequency dielectric constant, and $\omega_{TO,X}$ ($\omega_{LO,X}$) is the transverse optical (longitudinal optical) phonon angular frequency for the mode X, for each crystalline structure (cubic and hexagonal). Here X means either the irreducible representation of $A_1(z)$ (z-axis) or $E_1(xy)$ (xy-plane) at the Γ point.

Assuming that the hybrid wave is propagating in the x-direction with a phase velocity equal to ω/v_x, the solutions of equations (4) and (5) can be cast into the forms:

$$u_j = \alpha_j \exp(ikz)\exp(iq_x x - i\omega t), \quad j = x, y, z \tag{9}$$

$$\phi = \alpha_4 \exp(ikz)\exp(iq_x x - i\omega t), \tag{10}$$

where the α's coefficients are the amplitudes of the different components. Substitution of the solutions of equations (9) and (10) into the coupled equations (4) and (5) yields coupled differential equations for the pairs (u_x, u_z)

and (u_y, ϕ) for both symmetries (cubic and hexagonal), where in the latter the coupling is due to the piezoelectric tensor.

For the zinc-blende (cubic) structure, taking into account the appropriate form of the elastic and piezoelectric tensor [20], and considering only the piezoelectric case of interest to us, i.e. the pair (u_y, ϕ), these equations are reduced to:

$$-\rho\omega^2 u_y - C_{44}\left(\frac{\partial^2 u_y}{\partial z^2} + \frac{\partial^2 u_y}{\partial x^2}\right) - 2e_{x4}\frac{\partial^2 \phi}{\partial x \partial z} = 0 \quad (11)$$

$$2e_{x4}\frac{\partial^2 u_y}{\partial x \partial z} - \epsilon_{xx}\left(\frac{\partial^2 \phi}{\partial z^2} + \frac{\partial^2 \phi}{\partial x^2}\right) = 0, \quad (12)$$

where C_{44} and e_{x4} are the components of the elastic and piezoelectric tensors, respectively (from now on we will use the short notation C_{IJ} and e_{iJ} for simplicity). Solving these coupled equations we obtain (omitting the common $\exp(iq_x x)$ factor):

$$u_y = L(k_1)\Big[B_1 \exp(ik_1 z) - B_2 \exp(-ik_1 z)\Big] + (\epsilon_{xx}/e_{x4})L(k_2)\Big[B_3 \exp(ik_2 z) - B_4 \exp(-ik_2 z)\Big], \quad (13)$$

$$\phi = (e_{x4}/\epsilon_{xx})\Big[B_1 \exp(ik_1 z) + B_2 \exp(-ik_1 z)\Big] + \Big[B_3 \exp(ik_2 z) + B_4 \exp(-ik_2 z)\Big]. \quad (14)$$

Here B_r $(r = 1, 2, 3, 4)$ are unknowns coefficients to be determined through the boundary conditions, and $k_{1,2} = (k_{+,-})^{1/2}$, where

$$k_{\pm}^2 = \Big[q_{Tz}^2 - q_x^2(1 + 4p) \pm \Delta\Big]\Big/2. \quad (15)$$

Also,

$$\Delta = \left[\left(q_{Tz}^2 + q_x^2\right)^2 + 8q_x^2 p\left(2q_x^2 p - q_{Tz}^2 + q_x^2\right)\right]^{1/2}, \quad (16)$$

$$q_{Tz}^2 = \left(\omega/v_T\right)^2 - q_x^2, \quad (17)$$

$$L(k) = k\Big[k^2 + q_x^2(1 + 4p)\Big]\Big/\left(2q_x q_{Tz}^2\right). \quad (18)$$

In the above equations, $p = e_{x4}^2/\epsilon_{xx}C_{44}$, q_{Tz} (q_x) is the z- $(x$-)component of the transverse wavevector of the elastic wave, whose transverse velocity v_T is given by $v_T = (C_{44}/\rho)^{1/2}$. Observe that when the piezoelectric coupling is zero $(p = 0)$, equation (15) yields the limits $k_+^2 = q_{Tz}^2$ and $k_-^2 = q_x^2$, as it should be.

On the other hand, for the wurtzite (hexagonal) symmetry one finds:

$$-\rho\omega^2 u_y - C_{44}\left(\frac{\partial^2 u_y}{\partial z^2} + \frac{\partial^2 u_y}{\partial x^2}\right) - e_{x5}\left(\frac{\partial^2 \phi}{\partial z^2} + \frac{\partial^2 \phi}{\partial x^2}\right) = 0 \quad (19)$$

$$e_{x5}\left(\frac{\partial^2 u_y}{\partial z^2} + \frac{\partial^2 u_y}{\partial x^2}\right) - \epsilon_{xx}\left(\frac{\partial^2 \phi}{\partial z^2} + \frac{\partial^2 \phi}{\partial x^2}\right) = 0, \quad (20)$$

whose solutions are:

$$u_y = \Big[B_1' \exp(ikz) + B_2' \exp(-ikz)\Big]\exp(iq_x x),$$

$$\phi = \Big\{(e_{x5}/\epsilon_{xx})\Big[B_1' \exp(ikz) + B_2' \exp(-ikz)\Big] + B_3' \exp(q_x z) + B_4' \exp(-q_x z)]\Big\}\exp(iq_x x), \quad (21), (22)$$

with k given by

$$k^2 = \Big(q_{Tz}^2 - p' q_x^2\Big)\Big/(1 - p'), \quad (23)$$

and $p' = e_{x5}^2/\epsilon_{xx}C_{44}$.

Furthermore, considering in the sapphire layer that there is no coupling between the electromagnetic and the elastic waves, we have

$$u_y = \Big[A_1 \exp(iq_{Tz} z) + A_2 \exp(-iq_{Tz} z)\Big]\exp(iq_x x), \quad (24)$$

$$\phi = \Big[A_3 \exp(-q_x z) + A_4 \exp(q_x z)\Big]\exp(iq_x x). \quad (25)$$

In the next section we will use the expressions found for the elastic displacement u_y and the electrical potential ϕ to determine the phonons's dispersion relation using a suitable transfer-matrix approach.

3 Periodic and quasiperiodic superlattices

Now we turn to the binary superlattice /Al_2O_3/GaN/$\cdots$ /vacuum, considering first GaN with a cubic zinc-blende crystalline structure. The unit cell of the superlattice has thickness $L = d_a + d_b$, where d_a (d_b) is the thickness of the sapphire (GaN) layer. For the superlattice bulk modes, the coupled field equations, defined by equations (11) and (12), together with the elastic and electromagnetic boundary conditions at the nth unit cell, i.e., the interfaces $z = nL + d_a$ (Al_2O_3/GaN) and $z = (n + 1)L$ (GaN /Al_2O_3), yield:

(a) by imposing continuity of the transverse displacement u_y:

$$A_1^{(n)} f_a + A_2^{(n)} \bar{f}_a = L(k_1)\Big[B_1^{(n)} - B_2^{(n)}\Big] + p_2^{-1} L(k_2)\Big[B_3^{(n)} - B_4^{(n)}\Big] \quad (26)$$

$$A_1^{(n+1)} + A_2^{(n+1)} = L(k_1)\Big[B_1^{(n)} f_{b1} - B_2^{(n)} \bar{f}_{b1}\Big] + p_2^{-1} L(k_2)\Big[B_3^{(n)} f_{b2} - B_4^{(n)} \bar{f}_{b2}\Big]; \quad (27)$$

(b) by imposing continuity of the electrical potential ϕ:

$$A_3^{(n)} f_x + A_4^{(n)} \bar{f}_x = p_2\Big[B_1^{(n)} + B_2^{(n)}\Big] + B_3^{(n)} + B_4^{(n)}, \quad (28)$$

$$A_3^{(n+1)} + A_4^{(n+1)} = p_1\Big[B_1^{(n)} f_{b1} - B_2^{(n)} \bar{f}_{b1}\Big] + B_3^{(n)} f_{b2} + B_4^{(n)} \bar{f}_{b2}; \quad (29)$$

$$N_1 = \begin{pmatrix} L(k_1) & -L(k_1) & L(k_2)/p_2 & -L(k_2)/p_2 \\ k_1L(k_1) & k_1L(k_1) & k_2L(k_2)/p_2 & -k_2L(k_2)/p_2 \\ p_2 & p_2 & 1 & 1 \\ -i\epsilon_{xx}k_1p_2/\epsilon_s q_x & i\epsilon_{xx}k_1p_2/\epsilon_s q_x & -i\epsilon_{xx}k_2/\epsilon_s q_x & i\epsilon_{xx}k_2/\epsilon_s q_x \end{pmatrix}. \quad (44)$$

(c) by imposing continuity of the transverse stress tensor S_{32}:

$$q_{Tz}\mu\Big[A_1^{(n)}f_a - A_2^{(n)}\bar{f}_a\Big] - q_x p_1\Big[A_3^{(n)}f_x + A_4^{(n)}\bar{f}_x\Big] = L(k_1)k_1\Big[B_1^{(n)} + B_2^{(n)}\Big] + p_2^{-1}L(k_2)k_2\Big[B_3^{(n)} + B_4^{(n)}\Big] \quad (30)$$

$$q_{Tz}\mu\Big[A_1^{(n+1)} - A_2^{(n+1)}\Big] - q_x p_1\Big[A_3^{(n+1)} + A_4^{(n+1)}\Big] = L(k_1)k_1\Big[B_1^{(n)}f_{b1} + B_2^{(n)}\bar{f}_{b1}\Big] + p_2^{-1}L(k_2)k_2 \times \Big[B_3^{(n)}f_{b2} + B_4^{(n)}\bar{f}_{b2}\Big]; \quad (31)$$

(d) by imposing continuity of the normal component of the electrical displacement D_z:

$$A_3^{(n)}f_x - A_4^{(n)}\bar{f}_x = -\Big(i\epsilon_s/q_x\epsilon_{xx}\Big)\Big[p_2k_1\Big(B_1^{(n)} - B_2^{(n)}\Big) + k_2\Big(B_3^{(n)} - B_4^{(n)}\Big)\Big] \quad (32)$$

$$A_3^{(n+1)} - A_4^{(n+1)} = -\Big(i\epsilon_s/q_x\epsilon_{xx}\Big) \times \Big[p_2k_1\Big(B_1^{(n)}f_{b1} - B_2^{(n)}\bar{f}_{b1}\Big) + k_2\Big(B_3^{(n)}f_{b2} - B_4^{(n)}\bar{f}_{b1}\Big)\Big], \quad (33)$$

where ϵ_s is sapphire's dielectric constant. In the above equations we have used the following definitions:

$$f_m = \exp(iq_{Tz}d_m) = 1/\bar{f}_m, \quad m = a, b \quad (34)$$

$$f_x = \exp(-q_x d_a) = 1/\bar{f}_x \quad (35)$$

$$f_{br} = \exp(ik_r d_b) = 1/\bar{f}_{br}, \quad r = 1, 2 \quad (36)$$

$$p_1 = e_{x4}/C_{44(\mathrm{GaN})} \quad (37)$$

$$p_2 = e_{x4}/\epsilon_s \quad (38)$$

$$\mu = C_{44(\mathrm{GaN})}/C_{44(\mathrm{sapphire})}. \quad (39)$$

Defining the kets formed by the unknowns coefficients

$$|A^{(n)}\rangle = \begin{pmatrix} A_1^{(n)} \\ A_2^{(n)} \\ A_3^{(n)} \\ A_4^{(n)} \end{pmatrix}, \quad (40)$$

with similar expression for $|B^{(n)}\rangle$, equations (26) to (33) can be expressed as the matrices equations

$$M_1|A^{(n)}\rangle = N_1|B^{(n)}\rangle \quad (41)$$

$$M_2|A^{(n+1)}\rangle = N_2|B^{(n)}\rangle, \quad (42)$$

where

$$M_1 = \begin{pmatrix} f_a & \bar{f}_a & 0 & 0 \\ q_{Tz}\mu f_a & -q_{Tz}\mu\bar{f}_a & -q_x p_1 f_x & -q_x p_1\bar{f}_x \\ 0 & 0 & f_x & \bar{f}_x \\ 0 & 0 & f_x & -\bar{f}_x \end{pmatrix}, \quad (43)$$

and

see equation (44) above.

The matrix M_2 is obtained from M_1 by dividing the first row by f_a, the second by $\bar{f}_a$, the third by f_x, and the fourth by $\bar{f}_x$. Similarly, we can obtain the matrix N_2 from N_1 by multiplying the first row by f_{b1}, the second by $\bar{f}_{b1}$, the third by f_{b2}, and the fourth by $\bar{f}_{b2}$.

In a similar way we can carry out the case where GaN has a hexagonal wurtzite crystalline structure. The results are similar to those found for the cubic case: the matriz M_1' is identical to the matrix M_1 provided we replace the piezoelectric term p_1 by $p_1' = e_{x5}/C_{44}$, whereas the matrix N_1' is given by:

$$N_1' = \begin{pmatrix} 1 & 1 & 0 & 0 \\ k(1+p_1') & -k(1+p_1') & iq_x p_1' & -iq_x p_1' \\ p_2' & p_2' & 1 & 1 \\ 0 & 0 & \epsilon_{xx}/\epsilon_s & -\epsilon_{xx}/\epsilon_s \end{pmatrix}. \quad (45)$$

Furthermore, the matrix M_2' can be found in the same way as discussed in the cubic case. The matrix N_2' can be obtained from the matrix N_1' by multiplying the first row by $f_b = \exp(ikd_b)$, the second by $\bar{f}_b = 1/f_b$, the third by f_x, and the fourth by $\bar{f}_x$. Besides, p_1' and p_2' are defined as for p_1 and p_2, respectively, provided we replace e_{x4} by e_{x5}.

It is easy to show that, using equations (41) and (42) one can find:

$$|A^{(n+1)}\rangle = T|A^{(n)}\rangle = \exp(iQ_iL)|A^{(n)}\rangle, \quad (46)$$

where in the last step Bloch's ansatz was used. Here T, the so-called transfer matrix, is given by:

$$T = M_2^{-1}N_2N_1^{-1}M_1. \quad (47)$$

Therefore,

$$[T - \exp(iQ_iL)I]|A^{(n)}\rangle = 0, \quad (48)$$

where I is the identity matrix. Equation (48) is the secular equation defining the bulk phonon dispersion relation. Since T is an unimodular matrix ($\det T = 1$), its eigenvalue should satisfy $t_1t_2t_3t_4 = 1$, i.e., $t_2 = t_1^{-1}$ and

$t_4 = t_3^{-1}$. Therefore Bloch's wavevector should satisfy

$$\exp(iQ_rL) = t_r, \quad r = 1, 2. \tag{49}$$

If we truncate the superlattice at $z = 0$ (semi-infinite geometry), considering vacuum occupying the region $z < 0$ (stress free interface), straightforward calculation yield the following dispersion relation for the surface modes:

$$\begin{aligned}(T_{11} + T_{12} - T_{21} - T_{22})(T_{33} - T_{44} + T_{34}\lambda - T_{43}\lambda^{-1}) \\ + (T_{41} + T_{42})[(T_{13} - T_{23})\lambda^{-1} + (T_{14} - T_{24})] \\ - (T_{31} + T_{32})[T_{13} - T_{23} + (T_{14} - T_{24})\lambda] = 0.\end{aligned} \tag{50}$$

Here T_{ij} are elements of the transfer matrix T, and

$$\lambda = (\epsilon_{\text{vacuum}} + 1)/(\epsilon_{\text{vacuum}} - 1). \tag{51}$$

Now we present some numerical results to characterize the spectrum of the acoustic phonons (bulk and surface modes) that can propagate in the Al_2O_3/GaN periodic structures described above. The physical parameters used are:

(i) for GaN [21]: $\omega_{LO,E_1} = 94.06$, $\omega_{TO,E_1} = 73.22$, and $\epsilon_\infty = 5.29$; [22]: $\rho = 6.25$, $C_{44} = 1.54$, $e_{x4} = 0.73$, and $e_{x5} = 0.49$;
(ii) for Al_2O_3 [23]: $\epsilon_\infty = 10$, $\rho = 2.2$, $C_{44} = 3.12$,

where the frequencies are in units of meV, the elastic terms in units of 10^{11} N/m^2, the piezoelectric terms in units of C/m^2, and the densities in units of 10^3 kg/m^3. We have considered the thickness of the Al_2O_3 (sapphire) layer d_a equal to 10 nm, and the ratio $d_a/d_b = 0.5$. For numerical results, instead of to use the frequency ω, we prefer to replace it by the reduced frequency ω/Ω where $\Omega = v_T/d_a$.

The phonon spectra for the periodic superlattices, are presented in Figure 1, considering the cubic zinc-blende symmetry (Fig. 1a) and the hexagonal wurtzite one (Fig. 1b), respectively. In all these spectra the surface modes are represented by the dashed lines, while the bulk bands are characterized by the shadow areas. For the cubic case, depicted in Figure 1a, the bulk phonon spectrum has three well-defined branches in the range $0 < \omega/\Omega < 3.5$, with the surface modes between them. The highest-frequency surface branch is so closed to the bulk band that it is not visible in the scale used here. The second surface mode starts at $\omega/\Omega = 1.5$ and then merges into the bulk band at $\omega/\Omega \simeq 2.2$ for $q_x d_a \simeq 1.25$. The lowest-frequency surface mode merges from the bulk band at $q_x d_a = 0.25$ and then evolves quite apart of the bulk band. For the hexagonal case, on the other hand, the bulk spectra has now only two branches in the same range of frequency $0 < \omega/\Omega < 3.5$, with the surface modes so closed to the bulk bands that are not visible in the scale used here. Neglecting the piezoelectric coupling, the spectra (not shown here), although keeping some qualitative resemblance when compared with those shown in Figure 1, present a less pronounced curvature of the bulk bands (they are quite flat), leading to a smaller gap between them.

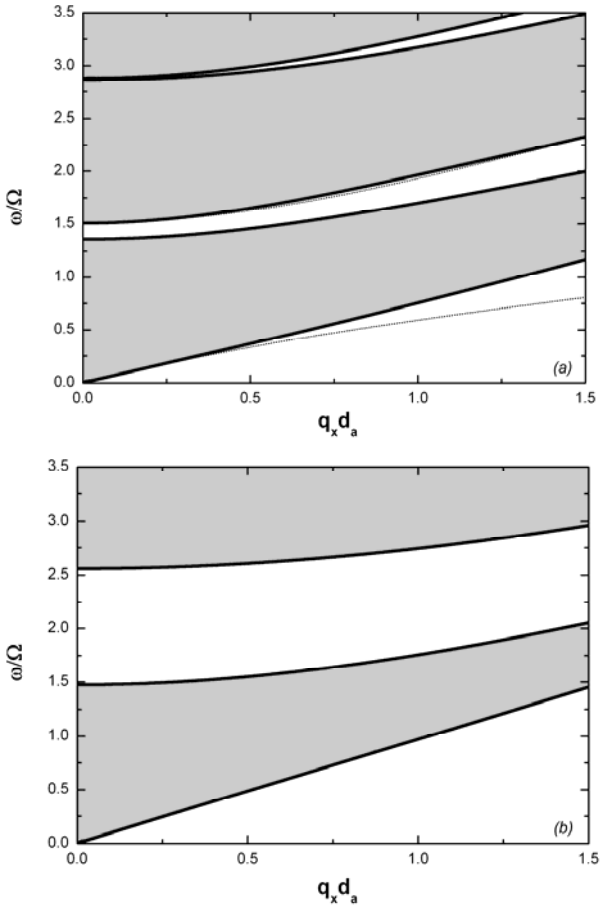

Fig. 1. Acoustic phonon's spectra for a periodic GaN/sapphire superlattice, measured by the reduced frequency ω/Ω, as a function of the dimensionless factor $q_x d_a$. Here the bulk bands are represented by the shadow areas, while the dashed lines defines the surface modes. (a) cubic zinc-blende symmetry; (b) hexagonal wurtzite symmetry.

We now turn our attention to the quasiperiodic structures. In order to construct them, we define briefly here the rules of the unit cell growth, that consists of a sequence of building blocks (or layers), where the arrangement of the layers follows the desired sequence. For the well-known Fibonacci (FB) sequence, the rule is $S_n = S_{n-1}S_{n-2}$, $n > 2$, where $S_1 = A$, $S_2 = AB$. The FB rule is invariant under the transformation $A \to AB$ and $B \to A$. Here A means the sapphire layer, while B represents the GaN one. These inflation rules can also be understood as an invariance condition, because they leave their respective sequences invariant when applied.

The Fibonacci generations are:

$$S_0 = [B]; S_1 = [A]; S_2 = [AB];, S_3 = [ABA] \quad \text{etc.} \tag{52}$$

The number of the building blocks increases according to the Fibonacci number, $F_l = F_{l-1} + F_{l-2}$ (with $F_0 = F_1 = 1$), and the ratio between the number of the building blocks A and the number of the building blocks B

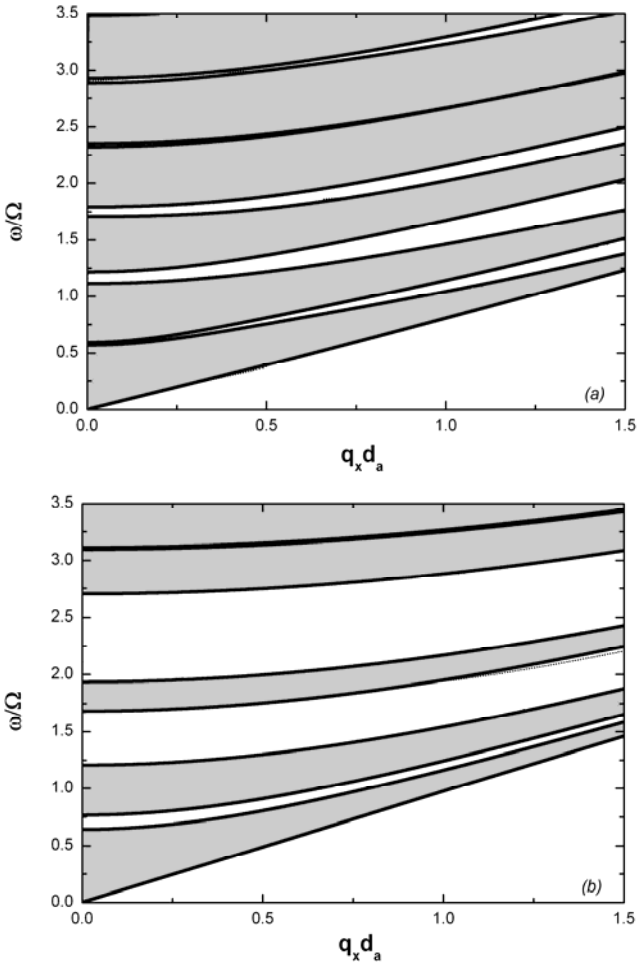

Fig. 2. Same as in Figure 1 but for the 4th generation Fibonacci quasiperiodic superlattice.

in the sequence is equal to the golden mean number $\tau = (1/2)(1+\sqrt{5})$.

To determine the phonon dispersion relation for the quasiperiodic FB structure we can use equations (48) and (50) with the appropriated transfer matrices, which for the zinc-blend cubic structure are given by:

(a) for $S_0 = [B]$ or $S_1 = [A]$

$$T_{S_0} = N_2^{-1} M_2; T_{S_1} = N_1^{-1} M_1; \tag{53}$$

(b) for $S_2 = [AB]$

$$T_{S_2} = N_1^{-1} M_2 N_2^{-1} M_1; \tag{54}$$

(c) for any higher generation ($k \geq 1$)

$$T_{S_{k+2}} = T_{S_k} T_{S_{k+1}}; \tag{55}$$

with a similar expression for the hexagonal wurtzite structure, provided we replace all cubic M's and N's matrices by their hexagonal counterparts. Therefore, from the knowledge of the transfer matrices T_{S_0}, T_{S_1}, and T_{S_2} we can determine the transfer matrix of any FB generation.

The phonon spectra for the quasiperiodic Fibonacci superlattices, considering its 4th generation number ($N = 4$), are presented in Figure 2, for the cubic zinc-blende symmetry (Fig. 2a) and the hexagonal wurtzite one (Fig. 2b), respectively, using the same physical parameters as for the periodic case. As in Figure 1, the surface modes are represented by the dashed lines, while the bulk bands are characterized by the shadow areas. For the cubic case, depicted in Figure 2a, the bulk phonon spectrum has six well-defined branches in the range $0 < \omega/\Omega < 3.5$, with the surface modes between them. This mean that one important effect of the quasiperiodicity was to split out the original three bulk branches found for the periodic case, and indeed in general, this behavior is found when the Fibonacci's generation number increases. A similar behavior was found also for the hexagonal wurtzite symmetry depicted in Figure 2b. Furthermore, the quasiperiodic spectra are more sensitive to the piezoelectric effect. Neglecting it, the spectra (not shown here), when compared to those shown in Figure 2, besides presenting a less pronounced curvature of the bulk bands, leading to a smaller gap between them (as in the periodic case), have a slight different number of bulk bands (and therefore changing also the number of surface modes which lie between them).

4 Localization profiles

One of the most fascinating aspects of excitations in quasiperiodic structures concerns their localizations and connections with fractal behavior. Keeping this in mind, we now proceed with an analysis of the acoustic phonon's confinement effects arising from competition between the long-range aperiodic order, which is induced by the quasiperiodic structure, and the short-range disorder, whose importance depends critically on the total length of the structure. To this end, a quantitative analysis will be made for the localization and magnitude of the allowed phonon's energy bandwidth in the phonon spectra, which were described in the previous section for the Fibonacci quasiperiodic structure. Also we shall discuss the related scaling behavior as a function of the number of generations of the sequences.

Taking the Fibonacci case, data for the distribution of the phonon's energy bandwidths measured as the reduced frequency ω/Ω are shown in Figure 3 for the dimensionless in-plane wavevector $q_x d_a = 1$, considering both symmetries (cubic, depicted in Fig. 3a, and hexagonal, shown in Fig. 3b). One can deduce the forbidden and allowed energy bands as a function of the generation number N up to the 6th generation of the Fibonacci sequence. We note that, as expected, the allowed band regions exhibit a fragmented energy spectrum for large N, as an indication of greater localization of the modes. In fact, the total width Δ of the allowed energy regions (which is known as the Lebesgue measure of the energy spectrum) decreases with N as the power law $\Delta \sim F_N^{-\delta}$. Here F_N is the Fibonacci number and the exponent δ (the the so-called *diffusion constant* of the spectra) is a function of the common in-plane wavevector

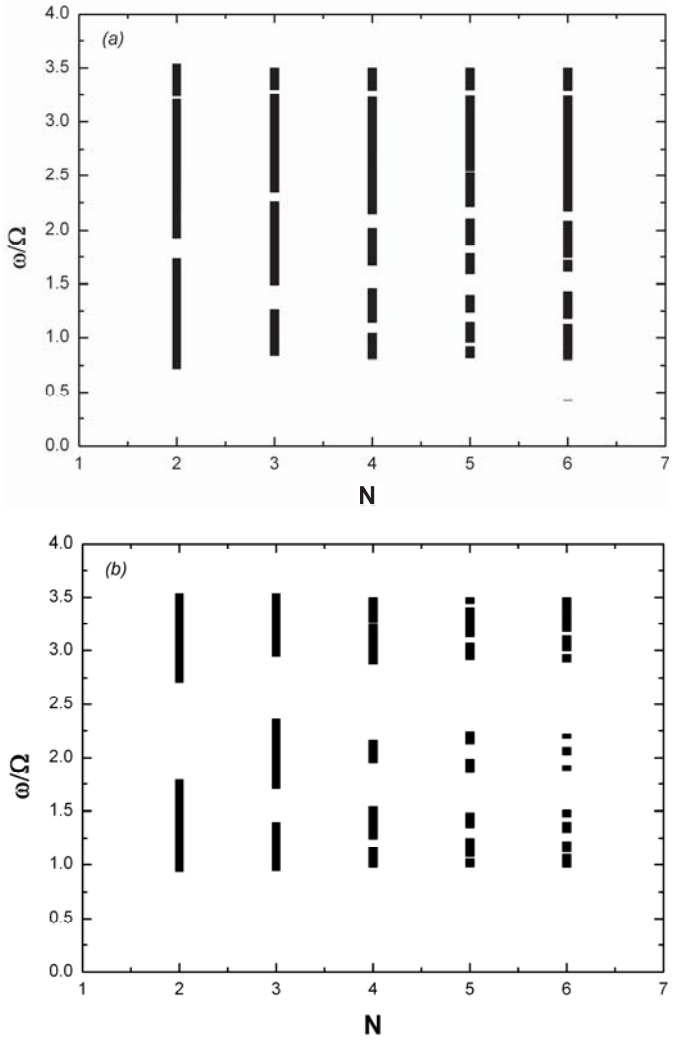

Fig. 3. The distribution of the acoustic phonon's energy bandwidths as a function of the quasiperiodic Fibonacci generation number N, considering the dimensionless in-plane wavevector $q_x d_a = 1.0$. (a) cubic zinc-blende symmetry; (b) hexagonal wurtzite symmetry.

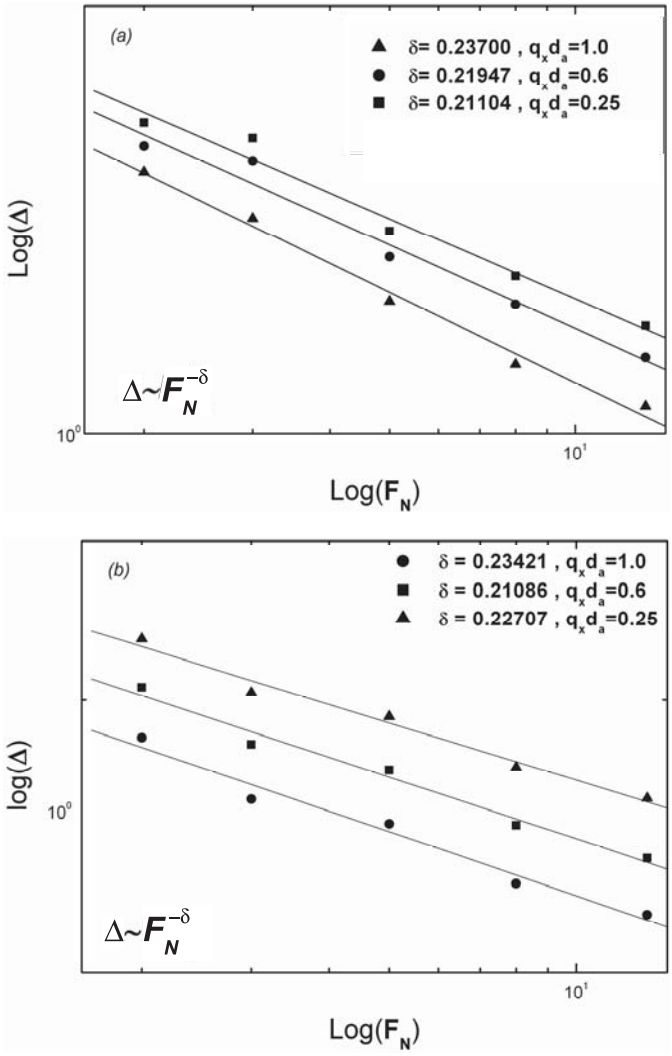

Fig. 4. Localization and scaling properties of the acoustic-phonon modes in the Fibonacci quasiperiodic structure, considering $N = 2$, 3, 4, 5 and 6. We have plotted $\mathrm{Log}(\Delta)$ against $\mathrm{Log}(F_N)$ for several values of the in-plane dimensionless wavevector $q_x d_a$ (see the legends, with δ indicating the slope of the curves). (a) Cubic zinc-blende symmetry; (b) hexagonal wurtzite symmetry.

$q_x d_a$. This exponent can be considered as indicating the degree of localization of the excitation [24]. In Figure 4 we show a log-log plot of these power laws for three different values of $q_x d_a$ (see the inset).

Have already proved that the acoustic phonon's energy spectra bandwidth in a Fibonacci quasiperiodic superlattice obey a linear scale law, which is a typical signature of a monofractal system (for details see Refs. [5,6]), let us analyze now its multifractal profile characterized by their $f(\alpha)$ spectrum. In this context, the study of the $f(\alpha)$ function is very important: it describes the distribution of different fractal dimensions of the object upon variation of the singularities of strength α [25].

A traditional method employed to determine the multifractal spectra, consists in defining a set of generalized dimensions D_g, whose associated spectrum of singularities $f(\alpha)$ is obtained through a Legendre transform [26]. Both of these quantities can be used to determine the whole spectra (for details see Ref. [27]). The difficulty of this method lies on the Legendre transform itself, depending on the system considered, and on eventual discontinuities that can arise on the $f(\alpha)$ curves [28].

A different approach for this problem, used in the present work, is based on some relationships between thermodynamic and multifractal formalisms [29], and was introduced by Chhabra and Jensen [30]. In this approach we first define our *measure*, namely the normalized local allowed bandwidth (Δ_i), i.e.

$$\chi_i = \frac{\Delta_i}{\sum_i \Delta_i}. \tag{56}$$

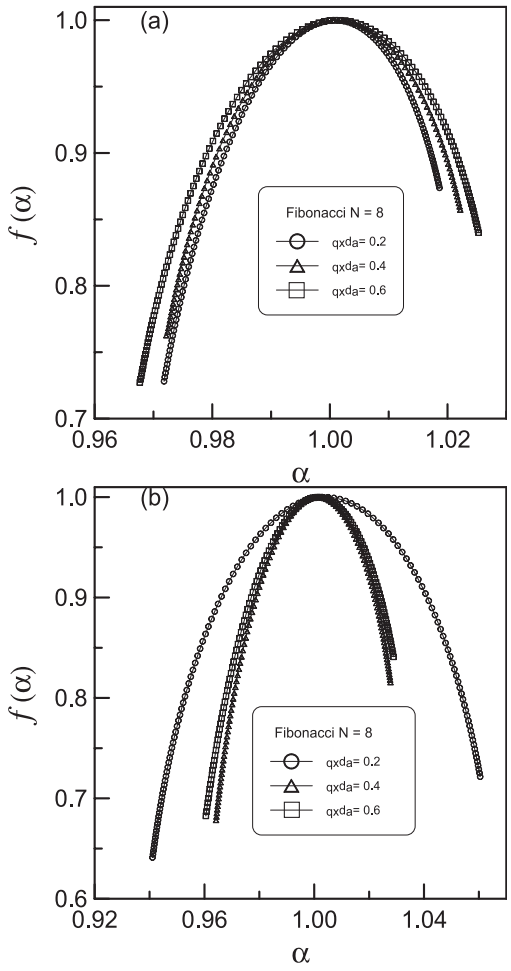

Fig. 5. The $f(\alpha)$ functions for the acoustic phonon's energy bandwidths, considering the 8th Fibonacci generation number and arbitrary values of the dimensionless in-plane wavevector $q_x d_a$. (a) Cubic zinc-blende symmetry; (b) hexagonal wurtzite symmetry.

The next step is to construct a parameterized family of these normalized measures:

$$\nu_i(g) = \frac{\chi_i^g}{\sum_i \chi_i^g}, \tag{57}$$

which are generalizations of the original measures χ_i. The multifractal spectrum $f(\alpha)$ is then obtained by varying the parameter g in equation (57) and calculating

$$f(\alpha_g) = \lim_{N\to\infty}\left[-\frac{\sum_i \nu_i \ln \nu_i}{\ln N}\right], \tag{58}$$

$$\alpha_g = \lim_{N\to\infty}\left[-\frac{\sum_i \nu_i \ln \chi_i}{\ln N}\right]. \tag{59}$$

In Figure 5 we show the $f(\alpha)$ functions for the 8th generation of the FB sequence, considering three different arbitrary values of the dimensionless in-plane wavevector $q_x d_a$, namely $q_x d_a = 0.2$, 0.4 and 0.6. For the cubic zinc-blende symmetry, one can notice that, differently from the multifractal Fibonacci spectra of magnetostatic modes [31], the curves are qualitatively insensitive for the dimensionless in-plane wavevector $q_x d_a$. The narrowing or the broadening of the curves are quantified by the *multifractal strength* of the system, which in turn is determined by the slope of each of the curves, given by the g exponents [26]. Quite different, for the hexagonal wurtzite symmetry, the curves are dependent to the dimensionless in-plane wavevector $q_x d_a$, mainly when $q_x d_a = 0.6$ onward.

For all cases the lower bound α_{min} and the upper bound α_{max} of the abscissa in the $f(\alpha)$ curves represent the minimum and maximum of the singularity exponent α, which acts as an appropriate weight in the reciprocal space. In fact, α_{min} and α_{max} characterize the scaling properties of the most concentrated and most rarified region of the intensity measure, respectively [30]. The value of $\Delta\alpha \equiv (\alpha_{max} - \alpha_{min})$ may be used as a parameter reflecting the randomness of the intensity measure, being bigger for the hexagonal wurtzite structure. Besides, the above multifractal analysis revealed a smooth $f(\alpha)$ function distributed in a finite range $[\alpha_{min}, \alpha_{max}]$ for both structures, with a summit at $f(\alpha_0) = 1$, indicating that the phonon spectra discussed here correspond to highly nonuniform intensity distributions, and therefore they possess the scaling properties of a multifractal.

In summary, we have described the spectra, localization and multifractal behavior for acoustic phonons propagating in periodic and quasiperiodic (Fibonacci type) semiconductor superlattices using a theoretical model beyond the elastic continuum approach. We have considered stacking of wurtzite and cubic semiconductor structures of GaN types surrounded by sapphire layers. The most important experimental technique used to probe these phonon modes is the Brillouin light scattering, and indeed it was previously been successfully applied for high-quality free-standing GaN substrate [32] as well as GaN thin film on sapphire substrate [33].

We would like to thank partial financial support from CNPq, CNPq-Edital Universal, CNPq-Rede NanoBioestruturas, FINEP-CTEnerg, FINEP-CTInfra and FAPEMA (Brazilian Research Agencies).

References

1. B. Gil, *Group III Nitride Semiconductor Compounds* (Clarendon, Oxford, 1998)
2. K.H. Ploog, O. Brandt, H. Yang, T. Trampert, Thin Solid Films, **306**, 231 (1997)
3. G. Ramirez-Flores, H. Navarro-Contreras, A. Lastras-Martinez, Phys. Rev. B **50**, 8433 (1994)
4. J.R.L. Fernandez, O.C. Noriega, J.A.N.T. Soares, F. Cerdeira, E.A. Meneses, J.R. Leite, D.J. As, D. Schikora, K. Lischka, Solid State Commun. **125**, 205 (2003)
5. E.L. Albuquerque, M.G. Cottam, Phys. Rep. **376**, 225 (2003)
6. E.L. Albuquerque, M.G. Cottam, *Polaritons in Periodic and Quasiperiodic Structures* (Elsevier, Amsterdam, 2004)
7. S.N. Zhu, Y.Y. Zhu, Y.Q. Qin, H.F. Wang, C.Z. Ge, N.B. Ming, Phys. Rev. Lett. **78**, 2752 (1997)

8. S.N. Zhu, Y.Y. Zhu, N.B. Ming, Science **27**, 8843 (1997)
9. M.E. Zoorob, M.D.B. Charlton, G.J. Parker, J.J. Baumberg, M.C. Netti, Nature **404**, 740 (2000)
10. F.A. Ponce, D. Cherns, W.T. Young, J.W. Steeds, Appl. Phys. Lett. **69**, 770 (1996)
11. T.L. Song, S.J. Chua, E.A. Fitzgerald, P. Chen, S. Tripathy, J. Vac. Sci. Technol. A **22**, 287 (2004)
12. F. Bernardini, V. Fiorentini, D. Vanderbilt, Phys. Rev. B **56**, R10024 (1997)
13. J. Gleize, J. Frandon, M.A. Renucci, F. Bechstedt, Phys. Rev. B **63**, 073308 (2001)
14. P.W. Mauriz, M.S. Vasconcelos, E.L. Albuquerque, Phys. Stat. Solidi (b) **243**, 1205 (2006)
15. J.E. Zarate, L. Fernandez-Alvarez, V.R. Velaco, Superlattices and Microsructures **25**, 519 (1999)
16. F. Garcia-Moliner, Ann. Phys. **2**, 179 (1977)
17. A. Nougaoui, B. Djafari-Rouhani, Surf. Sci. **185**, 154 (1987)
18. A. Bousfia, E.H. El Boudouti, D. Bria, A. Nougaoui, J. Appl. Phys. **87**, 4507 (2000)
19. B.A. Auld, *Acoustic Fields and Waves in Solids* (R.E. Krieger Publish Company, Malabar, Fl, 1990), Vols. 1 and 2
20. J.F. Nye, *Physical Properties of Crystals* (Clarendon, Oxford, 1985)
21. L.E. McNeil, M. Grimsditch, R.H. French, J. Am. Ceram. Soc. **76**, 1132 (1993)
22. F. Bechstedt, U. Grossner, J. Furthmüller, Phys. Rev. B **62**, 8003 (2000)
23. S.C. Jain, M. Willander, J. Narayan, R. Van Overstraeten, J. Appl. Phys. **87**, 965 (2000)
24. F. Dominguez-Adame, A. Sánchez, E. Diez, Phys. Rev. B **50**, 17736 (1994)
25. T.C. Halsey, M.G. Jensen, L.P. Kadanoff, I. Proccacia, B.I. Shraiman, Phys. Rev. A **33**, 1141 (1986)
26. T.C. Halsey, P. Meakin, I. Proccacia, Phys. Rev. Lett. **56**, 854 (1986)
27. G. Paladin, A. Vulpiani, Phys. Rep. **156**, 148 (1987)
28. P. Grassberger, R. Badii, A. Politi, J. Stat. Phys. **51**, 135 (1988)
29. M.H. Jensen, L.P. Kadanoff, I. Procaccia, Phys. Rev. Lett. **36**, 1409 (1987)
30. A.B. Chhabra, R.V. Jensen, Phys. Rev. Lett. **62**, 1327 (1989)
31. D.H.A.L. Anselmo, G.A. Farias, R.N. Costa and E.L. Albuquerque, Physica A **286**, 283 (2000)
32. M. Yamaguchi, T. Yagi, T. Sota, T. Deguchi, K. Shimada, S. Nakamura, J. Appl. Phys **85**, 8502 (1999)
33. M. Yamaguchi, T. Yagi, T. Azuhata, T. Sota, K. Suzuki, S. Chichibu, S. Nakamura, J. Phys.: Condens. Matter **9**, 241 (1997)